

SkinProfiler: Low-Cost 3D Scanner for Skin Health Monitoring with Mobile Devices

Zhiying Li

University of California, Los Angeles
Los Angeles, CA, USA
zhiyingli@ucla.edu

Zihan Yan

University of California, Los Angeles
Los Angeles, CA, USA
yzihan@mit.edu

Tejas Viswanath

University of California, Los Angeles
Los Angeles, CA, USA
tejasviswa@ucla.edu

Yang Zhang

University of California, Los Angeles
Los Angeles, CA, USA
yangzhang@ucla.edu

ABSTRACT

Melanoma is one of the top three most common skin cancers, originating from skin lesions and moles. Keeping track of skin lesion and mole developments in a precise and long-term manner has long been recommended but overlooked for the lack of accurate and easy-to-access tools. In response, we develop SkinProfiler, a low-cost mobile profiling tool for long-term skin health monitoring. To use SkinProfiler, users clamp an LED ring accessory onto smartphone cameras and take photos of the skin region of interest using the SkinProfiler app. Our modified photometric stereo algorithm leverages 17 photos taken with the skin surface lightened under various conditions to reconstruct 3D models of the skin surfaces. Our system stores 3D information for skin lesion and mole monitoring and diagnosis. The total cost of hardware assembly is under 20 dollars. We ran a preliminary evaluation to verify the performance of our tool. Based on the results, we propose several future steps including evaluations in clinical settings to complete this research.

CCS CONCEPTS

- Human-centered computing → Ubiquitous and mobile computing systems and tools.

KEYWORDS

Mobile Health, Smartphones, Skin Health, Photometric Stereo

ACM Reference Format:

Zhiying Li, Tejas Viswanath, Zihan Yan, and Yang Zhang. 2022. SkinProfiler: Low-Cost 3D Scanner for Skin Health Monitoring with Mobile Devices. In *Emerging Devices for Digital Biomarkers (DigiBiom '22)*, July 1, 2022, Portland, OR, USA. ACM, New York, NY, USA, 6 pages. <https://doi.org/10.1145/3539494.3542757>

Permission to make digital or hard copies of part or all of this work for personal or classroom use is granted without fee provided that copies are not made or distributed for profit or commercial advantage and that copies bear this notice and the full citation on the first page. Copyrights for third-party components of this work must be honored. For all other uses, contact the owner/author(s).

DigiBiom '22, July 1, 2022, Portland, OR, USA
© 2022 Copyright held by the owner/author(s).
ACM ISBN 978-1-4503-9406-2/22/07.
<https://doi.org/10.1145/3539494.3542757>

1 INTRODUCTION

Skin cancers are among the most common types of cancer [15]. In particular, malignant melanoma can be life-threatening if not detected early. Specifically, metastatic melanoma has a 5-year survival rate of approximately 10%. However, if it can be detected early, the 5-year survival rate increases to approximately 95% [34]. Melanoma is the main complication of moles and skin lesions. Most moles, brown spots, and growths on the skin remain harmless but can develop into metastatic melanoma. Therefore, it is essential and recommended to monitor moles and other skin lesions to look for changes in size, shape, or color.

In an out-of-clinic setting, people are recommended to use the ABCDE approach [30] and look for the ugly duckling sign [12], both of which rely on the naked eye. There have been imaging approaches to facilitate these processes by allowing users to take photos of skin regions of interest [2, 24, 37]. In clinical settings, dermatologists use dermoscopic camera systems, which are essentially high-resolution RGB cameras. These existing approaches only provide human-visible information and much depend on the examiners' experience. These approaches might be subjective and omit important information such as 3D shapes and thus can be prone to error (i.e., higher misclassification rates). Therefore, tools that can be easy to access, provide users with rich information, and work outside clinics to facilitate accurate skin self-examinations, are much needed.

In response, we created a mobile depth imaging tool geared toward skin self-examinations. Melanoma growth in the z-direction can be retrieved by sensing changes in the height with our tools. Our tool consists of an image acquisition phone accessory, algorithms built on the photometric stereo, and a visualization app. Collectively, we name our tool, SkinProfiler. In addition to RGB images of skin surfaces, our tool uniquely enables 3D depth sensing, allowing users to track shape changes of skin lesions and moles. In doing so, we create a new channel of information – depth, that users can rely on in self-examinations. We focus on depth information, commonly perceived as critical information in melanoma diagnosis. For instance, two metrics out of the five in the ABCDE approach involve checking on the depth information of skin surfaces (i.e., Asymmetry, and Evolving). Aligned with our effort are prior works that developed hyper-spectral imaging to provide dermatologists invisible information that cannot be provided by dermoscopic camera systems [17]. In addition, new raw sensing data can provide richer

feature sets as input and have the potential to enhance existing deep learning methods to aid melanomas diagnosis [13].

Our tool utilizes photometric stereo, which is a conventional technique for 3D reconstruction. Our work differs with prior work [27] in terms of innovation in using mobile phone camera as the image sensor to reduce the cost of the overall system and enhance the portability. By potentially turning billions of smartphones into skin profiling devices, our contributions include:

- (1) A compact and low-cost image acquisition phone accessory that features an LED ring for mobile uses.
- (2) A calibrated photometric stereo algorithm to retrieve the 3-dimensional geometry.
- (3) A visualization phone app that works in concert with the hardware and the algorithm to facilitate users' comprehension of the sensory data.
- (4) A preliminary evaluation that verifies the performance of our tool and suggests future steps.

2 RELATED WORK

2.1 Mobile Health Sensing

Smartphones, widely used and always available, provide an ideal platform for health sensing in our daily lives. Unlike using a self-customized attachment to sense and digitally communicate with the phone, built-in sensors are paid with more attention because of their more comprehensive application values. For example, Wang et al. developed "Seismo" to monitor blood pressure based on a built-in camera, and accelerometer [33]. With the development of computer vision, the camera has high potential value for integrating various medical functions into smartphones. For example, based on the smartphone camera, "Oralcam" enables self-examination of Oral Health [18]; "HemaApp" enables noninvasive blood screening of hemoglobin [32]; Chan et al. realizes pediatric vascular anomalies identifying with deep learning [4]. Skin-related Mobile Health research is also a important branch [5, 31].

2.2 Smartphone-based Skin Imaging

Although skin cancer is an increasing health issue, it is difficult for specialized health care professionals to implement population screening programs [8]. Thanks to the ubiquity of smartphone usage, smartphone-based skin imaging provides a more efficient way for more people to access early detection and surveillance of skin cancer [2, 8]. With the development of image-based computer-aided skin cancer diagnosis, there are already many intelligent skin healthcare apps that leverage the phone camera to retrieve user's skin information [16, 24, 37]. For example, the Miiskin app can monitor moles' numbers, positions, and sizes based on automatic skin imaging and mapping [22, 23]. SkinVision app is a smartphone app that expands users' ability to self-check moles and augments their knowledge about when and how to act [25]. Besides, some advanced mobile imaging algorithms further power the image processing of skin examining and mole screening [21]. However, most of them are based on 2D imaging, morphological evaluation [10] and machine learning [7, 29]. Furthermore, the clinical utility of deep learning models has yet to be demonstrated [38], and it is also difficult for users to comprehend.

2.3 Photometric Stereo Imaging

Photometric stereo is a 3D reconstruction method that recovers the orientation of the surface of objects using the observed intensity variations caused by illumination changes [1]. This working principle of this method is based on the fact that the amount of light reflected by a surface depends on the orientation of the surface relative to the light source and the observer [36]. Although the technique starts with the assumption that the object needs to be Lambertian [35], known point-like distant light sources, and uniform albedo [26], it has been expanded to various situations later, including non-Lambertian surface [6, 28]. Because the skin diffusely reflects incident light, it is somewhat Lambert reflective, enabling us to use the basic photometric stereo method.

The method requires at least three images obtained by lighting in different directions with the relative position of the camera and object unchanged. When collecting multiple images, the camera and the object must not be moved. Because the photometric stereoscopic method is based on the Woodham algorithm, it has some limitations. For one thing, it assumes that the camera is distortion-free. On the other hand, it is assumed that the beams emitted by each source are parallel and uniform.

3 IMPLEMENTATION

SkinProfiler mainly consists of three main components 1) a phone accessory, 2) a photometric stereo algorithm, and 3) a phone app.

3.1 Phone accessory

To use SkinProfiler, the accessory that we need is the image acquisition system, which is demonstrated in Figure 1(a). At the core of this accessory is an LED light dome that retrieves 16 illuminating conditions using this device. We use a phone camera macro lens, and we mount onto it a 3D printed dome with a ring of 16 LEDs controlled by Teensy 3.2. As a prerequisite to reducing ambient light's influence, we choose to use black materials to create a completely dark environment. The user shall use the clip and position the lens right on top of the mobile phone camera to use this part.

The LED light dome is assembled with Figure. 1(b.1-b.6). The camera clamp (Figure. 1(b.1)) clips everything on top of the phone camera. It uses the screw mechanism fixing the 25x macro lens (Figure. 1(b.3)), and the slider on the clamp can be used further to adjust the relative position of the lens and phone camera. Since a phone camera at a close distance (≤ 5 cm) induces an inability to focus, we used the 25x macro lens (Figure. 1(b.3)). This usage reduces the depth of field of the phone camera to around 2 - 4cm, which suits the need for close-range acquisition of skin images. To give an appropriate camera to object distance, we created a light dome (Figure. 1(b.6)). On its inner surface, 16 white LEDs (Figure. 1(b.6)) are positioned to create the illumination conditions for the photometric stereo algorithm. The sequence of 16 LEDs is controlled by Teensy 3.2 board (Figure. 1(b.4)). Lastly, the Teensy holder (Figure. 1(b.2)) is for cable management and fixing the Teensy board. All materials are easily accessible through online distributors and can be reproduced for less than 20 dollars.



Figure 1: (a) SkinProfiler (*top-left*) LED light dome front view, (*Middle*) LED light dome all LEDs on, (*top-right*) LED light dome side view, (*bottom-left*) the calibration tool, (*bottom-right*) usage of the calibration tool; (b) fabrication and accessory assembly
1.camera clamp, 2.teensy holder, 3.macro Lens (25x), 4.Teensy 3.2, 5.light dome, 6.white LED, 7.stainless steel ball, 8.ball holder.

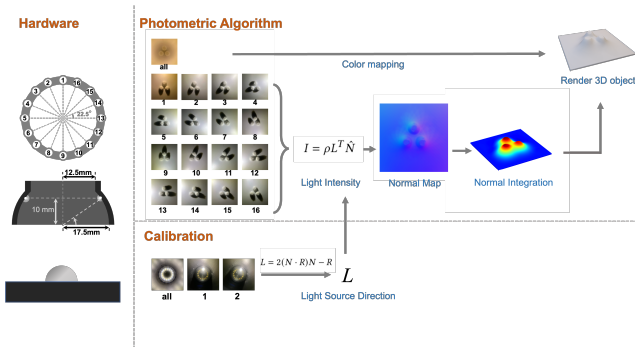


Figure 2: Our photometric stereo algorithm and calibration pipeline.

3.2 Algorithm

Figure 2 describes the pipeline for the photometric stereo algorithm. It mainly consists of two parts:

Generating Normal Maps: The first part consists of generating the normal map and albedo of the target skin patch. The main algorithm for the 3D surface reconstruction starts after the light directions for each of the LEDs on the LED ring are obtained through the calibration method (section 3.3). They are each treated as a point light source for now despite being close to the target because this deviation will be reduced to a certain extent in the post-processing step. As stated by Woodham [35] in classical photometric stereo, we first collect multiple images of the target area using different light sources (LEDs in our case) and stack them on top of each other. Using the classical formula of photometric stereo for an image with p pixels, we have:

$$I = \rho L^T \hat{N} \quad (1)$$

Where $I \in \mathbb{R}^{m \times p}$ and is the intensity vector which gives us the intensities measured from m light sources (which is 16 in our case), $L \in \mathbb{R}^{3 \times m}$ is the light direction matrix for m light sources in the 3 spatial dimensions, $\hat{N} \in \mathbb{R}^{3 \times p}$ is the surface normal at that pixel,

and ρ is the albedo of the target. We can then find the normal map using the pseudoinverse of L^T .

Normal Integration: The second part of the algorithm is to reconstruct the 3D model of the target skin patch using the obtained normal map. The normal map gives us the gradient of the target at each pixel which is then integrated using Discrete Poisson Normal Integration [14] with the following equation:

$$J(z) = \iint ((z_x - p)^2 + (z_y - q)^2) dx dy \quad (2)$$

Where z is the estimated depth function and p and q are the gradients with respect to x and y obtained using the normal map. The above equation is discretized using finite differences giving us a linear system $Ax = b$ with the x and b values corresponding to the stacked values of $z_{i,j}$ and given data $(p_{i,j}, q_{i,j})$. The A matrix gives the coefficients that arise from approximating the Laplace operator Δ [3]. Lastly, in order to enhance the performance of the solver, we precondition the linear system of equations with a matrix M that approximates A^{-1} . The modified system is given as:

$$MAx = Mb \quad (3)$$

This modified system gives better efficiency than the traditional solver as MA is now equivalent to the Identity matrix. The convergence speed of the iterative solver is much better, especially when A is a sparse matrix as it is in our case where the images are downsampled to a lower resolution (640×640) to improve the computation speed.

Additionally, to improve the overall reconstruction of the target area, we provide an artificial depth prior where we consider the edges of the target to be flat, as in most cases of skin profiling. This post-processing also helps with reducing the paraboloid type effect that the reconstruction of near light photometric stereo with classical photometric stereo produces [11].

3.3 Calibration

We fabricated a calibration tool for getting the exact LED position relative to the area of interest because we consider the error in

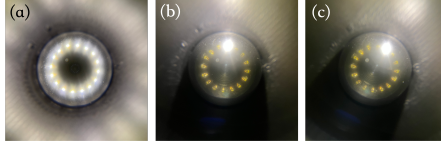


Figure 3: Example inputs for calibration (a) $t = 0$ image for getting all 16 LEDs' positions (b) $t = T$ image for recognizing the starting position (c) $t = 2T$ image for recognizing the direction of LEDs' illuminations.

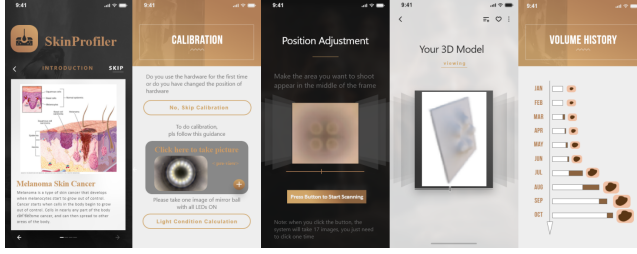


Figure 4: SkinProfiler workflow with UI design.

position caused by subtle differences in how people position the LED light domes. It consists of a metal ball with available sizes and a holder printed by a 3D printer. The calibration tool is assembled as is shown in Figure. 1(b.7,b.8). The stainless steel ball (Figure. 1(b.7)) is for reflecting the LEDs' illuminations during the calibration process. Knowing the real size of the stainless steel ball, we can also calibrate the pixel to real distance. The ball holder (Figure. 1(b.8)) is for revealing the hemisphere of the stainless steel ball so that the geometric center of the ball is aligned with the illumination center within the LED light dome.

In the calibration step, we take three images of a stainless steel ball with different LEDs ON in order to determine the light directions of the LEDs. These three images are essential to generating accurate light directions because of how the light directions change each time the hardware is clipped onto the mobile phone (i.e., the angle of rotation of the hardware is accounted). We estimate the radius and the coordinates of the center of the circle and then extract the locations of the specular highlights caused by the LEDs on this ball (brightest spots). The surface normals at these spots are then computed using the properties of a sphere. We can then use the geometry of Snell's Law for a reflective surface with $R = (0, 0, 1)$ as the viewing direction [9], and determine the light directions as in the following equation, with N being the surface normals.

$$L = 2(N \cdot R)N - R \quad (4)$$

3.4 Mobile App

Figure 4 shows the phone app of SkinProfiler. The *Introduction* page provides information on melanoma skin cancer, which can help the user understand what melanoma is, how detrimental it is to their health, and motivations of our system. There is also a *calibration* page that reminds the user to take a photo before using the hardware. Moreover, this picture will be used to correct the illumination

information. The *Position Adjustment* page allows users to view images captured by the phone's camera. Our app will remind users to adjust the position of the smartphone to make the mole appear in the center of the image. When users click the button to start scanning, the smartphone will take 17 images continuously according to the time interval of one photo per second. The *3D Model Demonstration* page enables the users to check the 3D structure of the mole. Users can view the 3D model from different angles by swiping gestures. Finally, the *Volume History* page visualizes the mole over the time axis, facilitating users to spot minute changes over time.

4 TECHNICAL EVALUATION

4.1 Setup and Procedure

We used an iPhone 13 in this evaluation. For the result of this paper, all pictures taken in this section were taken through the main camera of iPhone 13. Nonetheless, the purpose of this project is not phone specific. We do not focus on any particular tech specifications of any mobile phone cameras, and we do not make our engineering tailored toward iPhone 13. In the design process, we also tried other mobile phones within the lab with different levels of camera resolutions, and all those designs above are transferable to other devices.

To evaluate the effectiveness of the 3D reconstruction algorithm, we printed simple 3D semi-sphere geometry patterns to simulate moles on the skin. 3D printed geometry gives us the knowledge of the ground truth of the testing objects, so the evaluation process is numerical. In Figure. 5(a), we took two experiments to see (1) how results will vary if we change the sizes of the semi-spheres and (2) how results will vary if we change the quantity of the semi-spheres. For test 1, besides a blank surface, the resting 7 examples were semi-sphere with radius increases every 0.5mm starting from 1.5mm. For test 2, all semi-spheres were of radius 2 mm, and the quantities ranged from two to nine, and the semi-spheres were arranged in a compact and straightforward manner. For the experiments, We conducted 5 trials on each case, and each trial lasted around 60 - 90 seconds.

4.2 Results and Discussions

We report the error of depth of each surface mesh for our experiments, which means we quantify the differences between the reconstructed 3D models and the test surfaces as an average point-wise difference between the recovered height map and the ground truth height map. For our depth evaluation, only the pixels with valid depths in both ground truth and the reconstructed depth map will be involved in error calculation.

The recovered surface (Figure. 5(b)) can be represented by a normalized the height map $Z \in \mathbb{R}^{m \times n}$ with elements' values in between 0 and 1. We then normalized the known ground truth $Z_0 \in \mathbb{R}^{m \times n}$ to be $\bar{Z}_0 \in \mathbb{R}^{m \times n}$. The point-wise error rate is $\epsilon_{i,j} = |Z_{ij} - \bar{Z}_{0ij}|$, and the error rate is represented by $\epsilon_{av} = \frac{1}{m \times n} \sum_{i,j} \epsilon_{i,j}$.

Qualitatively, Figure. 5(b) demonstrates that the algorithm can distinguish the sizes and quantities of the semi-sphere patterns. The recovered surfaces maintain the same convexity with respect to the ground truth. From Figure. 5(d), the largest differences between the

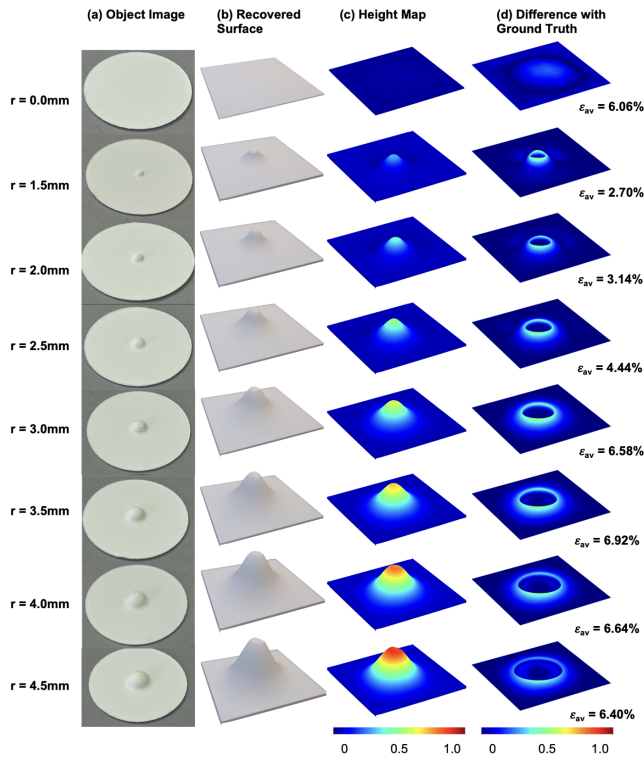
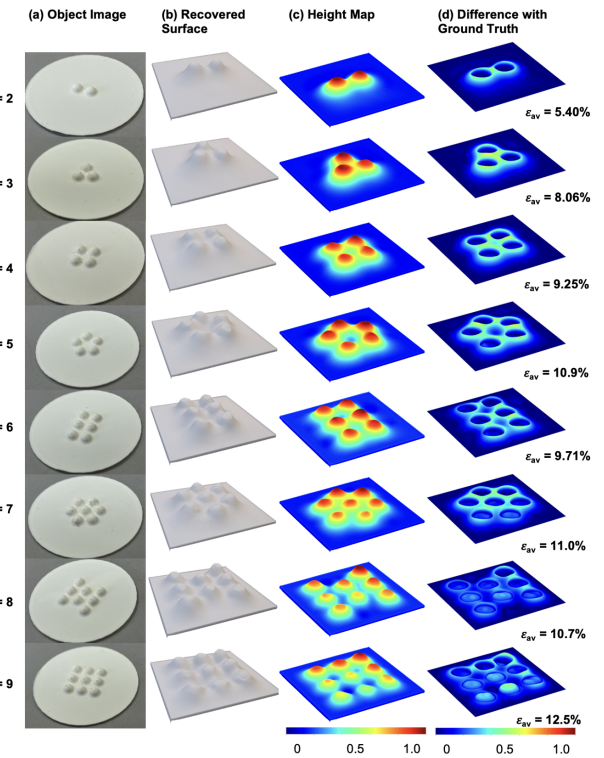
Test 1. change the size**Test 2. change the quantity**

Figure 5: Object images, recovered surfaces, height maps, point-wise differences and error rates; (test 1) one semi-sphere of radius from 1.5 to 4.5mm, and a flat surface as a comparison; (test 2) 2.0mm radius semi-spheres with quantity from 2 to 9.

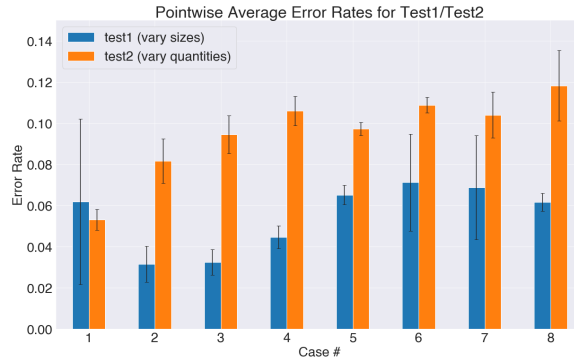


Figure 6: Average value across five trials: point-wise average error rates for test 1 (blue) and test 2 (orange).

recovered surface and the ground truth all happen at the edge of the semi-sphere.

Quantitatively, Figure. 6 records averaged error rates across 5 trials on the test cases. As we can see, the algorithm achieves the error rate of 2% - 14%. Interestingly, comparing test 1 and test 2, we found our algorithm performs overall better in a single semi-sphere. Also, for both tests, the algorithm performs worse as the regions for 3D geometry increase.

Currently, our algorithm could only yield smooth and continuous reconstructions (even if there is a sudden change in depth value) due to the nature of discrete Poisson integration. As the number of the features and contours increases, the consistency of heights across the reconstruction decreases, giving us slightly erroneous values. These deviations can be reduced to a certain extent when the regions of interest are isolated and reconstructed separately.

Our system is relatively good at distinguishing and tracking the bulk shapes, yet there is still room for improvement for detailed texture recovery. With higher fidelity in reconstructions, the system could meet requirements for clinical usages, which we plan to investigate in the future. In the current design, we have only applied a basic version of photometric stereo, which is constrained by simplified priors. Future work will explore advanced photometric stereo models, which have been proven successful in prior works [19, 20].

To validate our system clinically, we will run user studies by collaborating with medical professionals in the follow-up research. We would like to explore how to use SkinProfiler to support long-term skin health monitoring and telemedicine. We also plan to use SkinProfiler as a platform to investigate the interpretability and explainability of the result to let those without medical knowledge easily understand their skin health status. For example, we can quantify the 3D shape and assess the possibility of melanoma based

on AI models explained by easy-to-understand visualizations. These efforts would further extend the reach of the proposed system to a wider group of users for real-world impacts.

5 CONCLUSION

We present SkinProfiler, an end-to-end skin profiling system that leverages photometric stereo in mobile settings to reconstruct and keep track of 3D geometries of skin lesions and moles. The proposed system aims to facilitate users with a more flexible and easy-to-access way to self-examine early signs of melanoma, enabling long-term out-of-clinic skin health monitoring. We built SkinProfiler out of 1) a photo accessory with a dome that features 16 LEDs, 2) a photometric algorithm with its calibration process, and 3) a mobile app that visualizes the sensory data and facilitates users' comprehension of the data. A series of technical evaluations have pointed us to future work to improve the system for real-world user applications and evaluations.

REFERENCES

- [1] Jens Ackermann and Michael Goesele. 2015. A survey of photometric stereo techniques. *Foundations and Trends® in Computer Graphics and Vision* 9, 3-4 (2015), 149–254.
- [2] Abderrahim Bourouis, Ali Zerdazi, Mohammed Feham, and Abdelhamid Bouchachia. 2013. M-health: skin disease analysis system using Smartphone's camera. *Procedia Computer Science* 19 (2013), 1116–1120.
- [3] Michael Breuß, Yvain Quéau, Martin Bähr, and Jean-Denis Durou. 2016. Highly Efficient Surface Normal Integration.
- [4] Justin Chan, Sharat Raju, Randall Bly, Jonathan A Perkins, and Shyamnath Golakota. 2019. Identifying Pediatric Vascular Anomalies With Deep Learning. *arXiv preprint arXiv:1909.07046* (2019).
- [5] Elizabeth Chao, Chelsea K Meenan, and Laura K Ferris. 2017. Smartphone-based applications for skin monitoring and melanoma detection. *Dermatologic clinics* 35, 4 (2017), 551–557.
- [6] Guanying Chen, Kai Han, Boxin Shi, Yasuyuki Matsushita, and Kwan-Yee Kenneth Wong. 2020. Deep photometric stereo for non-Lambertian surfaces. *IEEE Transactions on Pattern Analysis and Machine Intelligence* (2020).
- [7] A Dascalu, BN Walker, Y Oron, and EO David. 2021. Non-melanoma skin cancer diagnosis: a comparison between dermoscopic and smartphone images by unified visual and sonification deep learning algorithms. *Journal of cancer research and clinical oncology* (2021), 1–9.
- [8] Tiago M de Carvalho, Eline Noels, Marlies Wakkee, Andreea Udrea, and Tamar Nijsten. 2019. Development of smartphone apps for skin cancer risk assessment: progress and promise. *JMIR Dermatology* 2, 1 (2019), e13376.
- [9] Paul Debevec. 1998. Rendering Synthetic Objects into Real Scenes: Bridging Traditional and Image-Based Graphics with Global Illumination and High Dynamic Range Photography. In *Proceedings of the 25th Annual Conference on Computer Graphics and Interactive Techniques (SIGGRAPH '98)*. Association for Computing Machinery, New York, NY, USA, 189–198. <https://doi.org/10.1145/280814.280864>
- [10] Ronald Dendere, Tinases Mutsvanga, Rene Goliath, Molebogeng X Rangaka, Ibrahim Abubakar, and Tania S Douglas. 2017. Measurement of skin induration size using smartphone images and photogrammetric reconstruction: pilot study. *JMIR Biomedical Engineering* 2, 1 (2017), e3.
- [11] Hao Fan, Lin Qi, Nan Wang, Junyu Dong, Yijun Chen, and Hui Yu. 2017. Deviation correction method for close-range photometric stereo with nonuniform illumination. *Optical Engineering* 56, 10 (2017), 1 – 13. <https://doi.org/10.1117/1.OE.56.10.103102>
- [12] Skin Cancer Foundation. 2022. Melanoma Warning Signs. <https://www.skincancer.org/skin-cancer-information/melanoma/melanoma-warning-signs-and-images/> Retrieved January 13, 2022.
- [13] Yunhao Ge, Bin Li, Yanzheng Zhao, Enguang Guan, and Weixin Yan. 2018. Melanoma Segmentation and Classification in Clinical Images Using Deep Learning. In *Proceedings of the 2018 10th International Conference on Machine Learning and Computing (Macau, China) (ICMLC 2018)*. Association for Computing Machinery, New York, NY, USA, 252–256. <https://doi.org/10.1145/3195106.3195164>
- [14] github.com. 2020. Discrete Normal Integration Github. <https://github.com/gray0018/Discrete-normal-integration> Normal Integration by solving a discrete object.
- [15] Gery P Guy Jr, Cherryl C Thomas, Trevor Thompson, Meg Watson, Greta M Massetti, and Lisa C Richardson. 2015. Vital signs: melanoma incidence and mortality trends and projections—United States, 1982–2030. *MMWR. Morbidity and mortality weekly report* 64, 21 (2015), 591.
- [16] Nazia Hameed, Anglia Ruskin, Kamal Abu Hassan, and M Alamgir Hossain. 2016. A comprehensive survey on image-based computer aided diagnosis systems for skin cancer. In *2016 10th International Conference on Software, Knowledge, Information Management & Applications (SKIMA)*. IEEE, 205–214.
- [17] Thomas Haugland Johansen, Kajsa Møllerse, Samuel Ortega, Himar Fabelo, Aday Garcia, Gustavo M Callico, and Fred Godtliebsen. 2020. Recent advances in hyperspectral imaging for melanoma detection. *Wiley Interdisciplinary Reviews: Computational Statistics* 12, 1 (2020), e1465.
- [18] Yuan Liang, Hsuan Wei Fan, Zhujun Fang, Leiyi Miao, Wen Li, Xuan Zhang, Weibin Sun, Kun Wang, Lei He, and Xiang'Anthony' Chen. 2020. OralCam: enabling self-examination and awareness of oral health using a smartphone camera. In *Proceedings of the 2020 CHI Conference on Human Factors in Computing Systems*. 1–13.
- [19] Fotios Logothetis, Roberto Mecca, and Roberto Cipolla. 2017. Semi-Calibrated Near Field Photometric Stereo. In *2017 IEEE Conference on Computer Vision and Pattern Recognition (CVPR)*. 4521–4530. <https://doi.org/10.1109/CVPR.2017.481>
- [20] Giljoo Nam and Min H. Kim. 2014. Multispectral Photometric Stereo for Acquiring High-Fidelity Surface Normals. *IEEE Computer Graphics and Applications* 34, 6 (2014), 57–68. <https://doi.org/10.1109/MCG.2014.108>
- [21] Hossein Nejati, Victor Pomponi, Thanh-Toan Do, Yiren Zhou, Sahar Iravani, and Ngai-Man Cheung. 2016. Smartphone and mobile image processing for assisted living: Health-monitoring apps powered by advanced mobile imaging algorithms. *IEEE Signal Processing Magazine* 33, 4 (2016), 30–48.
- [22] Alexander Ngoo, Anna Finnane, Erin McMeniman, H Peter Soyer, and Monika Janda. 2018. Fighting melanoma with smartphones: a snapshot of where we are a decade after app stores opened their doors. *International journal of medical informatics* 118 (2018), 99–112.
- [23] Nikos Petrellis. 2018. A review of image processing techniques common in human and plant disease diagnosis. *Symmetry* 10, 7 (2018), 270.
- [24] TE Sangers, M Wakkee, EC Kramer-Noels, T Nijsten, and M Lugtenberg. 2021. Views on Mobile Health Apps for Skin Cancer Screening in the General Population: An In-Depth Qualitative Exploration of Perceived Barriers and Facilitators. *British Journal of Dermatology* (2021).
- [25] Nivedita Singh and Shailendra K Gupta. 2019. Recent advancement in the early detection of melanoma using computerized tools: An image analysis perspective. *Skin Research and Technology* 25, 2 (2019), 129–141.
- [26] JA Smith, Tzeu Lie Lin, KJ Ranson, et al. 1980. The Lambertian assumption and Landsat data. *Photogrammetric Engineering and Remote Sensing* 46, 9 (1980), 1183–1189.
- [27] L.N. Smith, M.L. Smith, A.R. Farooq, J. Sun, Y. Ding, and R. Warr. 2011. Machine vision 3D skin texture analysis for detection of melanoma. *Sensor Review* 31, 2 (March 2011), 111–119. <https://doi.org/10.1108/0260228111109961>
- [28] Hemant D Tagare and Rui JP de Figueiredo. 1991. A Theory of Photometric Stereo for a Class of Diffuse Non-Lambertian Surfaces. (1991).
- [29] Muhammad Aleem Taufiq, Nazia Hameed, Adeel Anjum, and Fozia Hameed. 2017. m-Skin Doctor: A mobile enabled system for early melanoma skin cancer detection using support vector machine. In *eHealth 360°*. Springer, 468–475.
- [30] Hensin Tsao, Jeannette M Olazagasti, Kelly M Cordoro, Jerry D Brewer, Susan C Taylor, Jeremy S Bordeaux, Mary-Margaret Chren, Arthur J Sober, Connie Teiger, Reva Bhushan, et al. 2015. Early detection of melanoma: reviewing the ABCDEs. *Journal of the American Academy of Dermatology* 72, 4 (2015), 717–723.
- [31] Emily Vardell and Carmen Bou-Crick. 2012. VisualDx: a visual diagnostic decision support tool. *Medical reference services quarterly* 31, 4 (2012), 414–424.
- [32] Edward Jay Wang, William Li, Doug Hawkins, Terry Gernsheimer, Colette Norby-Slycord, and Shwetak N Patel. 2016. HemaApp: noninvasive blood screening of hemoglobin using smartphone cameras. In *Proceedings of the 2016 ACM International Joint Conference on Pervasive and Ubiquitous Computing*. 593–604.
- [33] Edward Jay Wang, Junyi Zhu, Mohit Jain, Tien-Jui Lee, Elliot Saba, Lama Nachman, and Shwetak N Patel. 2018. Seismo: Blood pressure monitoring using built-in smartphone accelerometer and camera. In *Proceedings of the 2018 CHI conference on human factors in computing Systems*. 1–9.
- [34] WIRES Authors. 2020. Detecting skin cancer using hyperspectral images. <https://www.advancedsciencenews.com/detecting-skin-cancer-using-hyperspectral-images/> Retrieved January 08, 2022.
- [35] Robert J Woodham. 1980. Photometric method for determining surface orientation from multiple images. *Optical engineering* 19, 1 (1980), 191139.
- [36] Ying Wu. 2003. Radiometry, brdf and photometric stereo. *Northwestern University* (2003).
- [37] Qahtan M Yas, AA Zaidan, BB Zaidan, M Hashim, and Chen Kim Lim. 2018. A systematic review on smartphone skin cancer apps: coherent taxonomy, motivations, open challenges and recommendations, and new research direction. *Journal of Circuits, Systems and Computers* 27, 05 (2018), 1830003.
- [38] Albert T Young, Niki B Vora, Jose Cortez, Andrew Tam, Yildiray Yeniyay, Ladi Afifi, Di Yan, Adi Nosrati, Andrew Wong, Arjun Johal, et al. 2021. The role of technology in melanoma screening and diagnosis. *Pigment Cell & Melanoma Research* 34, 2 (2021), 288–300.